

EFFECT OF PROCESSING ON THE HIGH TEMPERATURE LOW CYCLE FATIGUE PROPERTIES OF MODIFIED 9Cr-1Mo FERRITIC STEEL

G. EBI¹ and A. J. McEvily²

¹Max-Planck-Institut für Eisenforschung, Düsseldorf, West Germany and

²Department of Metallurgy, University of Connecticut, Storrs, CT 06268,

(Received in final form 30 April 1984)

Abstract-The high temperature low cycle fatigue properties of modified 9Cr-1Mo ferritic steel in a hot forged and a hot rolled condition have been evaluated. The hot forged material exhibited inferior fatigue properties as compared to the finer grained hot rolled material. Analysis of the data indicates that a larger grain size adversely affects the initiation stage but has little effect on the propagation stage. A steeper slope on the Coffin-Manson plot results when the number of cycles to initiation is reduced.

INTRODUCTION

The method of processing an alloy can be expected to have an effect on the high temperature low cycle fatigue (HTLCF) properties if different grain sizes and microstructures result as a consequence of different processing procedures. In this paper the effect of hot forging as compared to hot rolling of modified 9Cr-1Mo ferritic steel alloy is discussed. To establish the effect of the environment on HTLCF behaviour specimens of the hot rolled material were tested in vacuum. Metallurgical analyses were used to determine the nature of micro structural changes induced by HTLCF. A fractographic analysis was made to determine the rate of fatigue crack growth and the results were compared with predictions based upon a crack-opening displacement model for fatigue crack growth. The results of this investigation are detailed herein.

MATERIALS

Modified 9Cr-1Mo alloy was obtained from the Oak Ridge National Laboratories in plate form in both a hot rolled and a hot forged condition. The compositions of each plate are given in Table 1. In each case the material was normalized at 1038°C for 1 h, air cooled to room temperature and tempered for 1 h at 760°C after processing. Hot forging was done in the 1100-1150°C range; hot rolling at a lower range.

Modified 9Cr-1Mo alloy is a weld able ferritic steel of excellent harden ability and a desired level of elevated temperature properties, and an extensive compilation of its characteristics is available in Ref. [1]. The alloy contains small amounts of niobium (0.06-0.10 wt%) and vanadium (0.18-0.25 wt%). The niobium improves the properties by promoting the nucleation of a fine distribution of $M_{23}C_6$ [2] and by refining the grain size [3], whereas the vanadium enters the carbides and retards their growth [2]. Tempering 1-2 h at temperatures of 700-760°C after normalizing leads to the formation of $M_{23}C_6$ along prior austenitic grain boundaries and lath-martensite boundaries.

G. EBI and A. J. McEvily

Table 1. Chemical compositions of modified 9Cr-1Mo steels (wt%)

Element	Hot forged	Hot rolled
C	0.088	0.084
Cr	8.47	8.57
Mo	0.88	1.02
V	0.21	0.20
Nb	0.07	0.07
Mn	0.37	0.46
Si	0.19	0.40
Ni	0.09	0.09
P	0.011	0.010
S	0.004	0.003
N	0.054	0.053
Ti	0.001	0.005
Co	0.017	0.055
W	0.01	0.05

The microstructures for each condition are shown in Fig. 1. The microstructures consist of tempered martensite and show a coarser structure for the hot forged material. The prior austenite grain size characterized by the mean linear intercept were 31 μm for the hot forged material and 19 μm for the hot rolled material. No influence of the rolling direction on the microstructure of the hot rolled material was observed. As will be shown the grain size difference has a significant effect on HTLCF. The mechanical properties for each condition at 25 and 538°C are given in Table 2.

SPECIMENS AND TESTS

Mechanical testing

Thread-end specimens of cylindrical test sections and reduced diameter were employed, the test sections being 23.1 mm long and 7.62 mm in diameter. High temperature low cycle fatigue testing was carried out in an MTS servo hydraulic fatigue test machine equipped with a Lepel induction heater to provide the required test temperature of 538°C. The temperature was controlled to within $\pm 2^\circ\text{C}$ by a thermocouple located at the bottom shoulder of the gage section. The MTS was also equipped with a vacuum chamber and a pumping system that was able to provide a vacuum of 4×10^{-5} Torr.

Axial strain-controlled fatigue tests were performed in air and vacuum at 538°C using fully reversed sinusoidal strain waves of controlled total strain amplitude. The axial displacement was measured by a 23.1 mm gage-length extensometer. All tests were carried out under continuous cycling at a frequency of 0.1 Hz. At this frequency the temperature in the gage section remained constant, i.e. no magnetostrictive effect on temperature [4] which can occur at lower frequencies was observed in this particular specimen design.

Failure of a low cycle fatigue specimen is often defined as the point at which a 5% decrease occurs in the peak tensile stress as measured from the saturated stress amplitude. However, in the HTLCF tests of modified 9Cr-1 Mo materials a saturated stress amplitude was not observed. Instead, a period of gradual softening preceded a precipitous drop in maximum nominal stress which corresponded to the onset of macroscopic crack growth. Since during this period the stress range, $\Delta\sigma$, decreased linearly with an increasing number

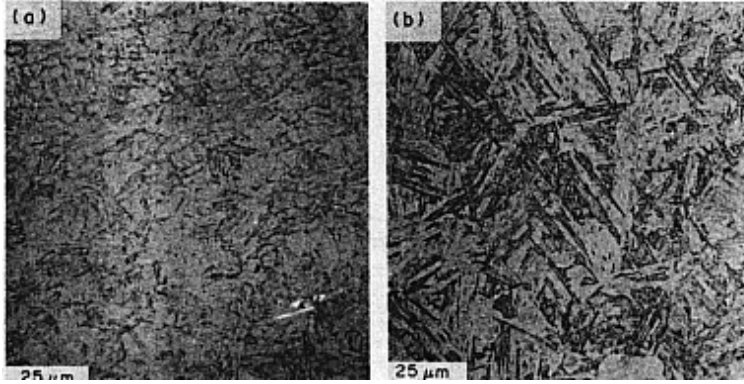


Fig. 1. Microstructures of (a) hot rolled and (b) hot forged modified 9Cr-1Mo steel.

of cycles N , failure of a specimen was defined by the following graphical procedure: (1) a line was drawn parallel to the linear portion of the $\Delta\sigma-N$ curve but offset from the original curve by 5% of the original stress range. (2) The intersection of the $\Delta\sigma-N$ curve and the offset line defined the number of cycles to failure.

Microscopy and analysis

Microstructures of samples in the as-received condition and after testing were examined by both optical and electron microscopy. The martensitic microstructures were revealed by a ferric chloride solution (10 g FeCl_3 , 23 ml HCl , 100 ml H_2O). The prior austenite grain boundaries were revealed by a special etchant developed by Enomoto *et al.* [5].

A Cambridge Stereoscan SEM was used to study HTLCF fracture surfaces and a Phillips EM 300 transmission electron microscope was used to examine thin foils. Transmission electron micrographs of the as received and fatigued samples were obtained from transverse cross-sections cut from the gage length portion of the low cycle fatigue specimens.

Samples of the carbide particles were anodically extracted from the as received material and from the gage section of fatigued specimens using a procedure similar to the one described by Leitnaker *et al.* [6]. X-ray analysis was performed on powder samples prepared from the extracted carbides and the modified 9Cr-1Mo materials. Powder diffraction patterns were obtained with a Debye-Scherrer camera using Cr-K α -radiation.

RESULTS

Cyclic stress response

Both materials showed rapid initial softening followed by gradual softening until macroscopic crack growth occurred (Fig. 2a and b). A comparison of the stress response

G. EBI and A. J. MCEVILY

Table 2. Mechanical properties of modified 9Cr-1Mo steels

Condition	Yield strength (MPa)		Tensile strength (MPa)			Elongation (%)			Reduction of area (%)			Hardness*		
	$T = 25^\circ\text{C}$	$T = 538^\circ\text{C}$	$T = 25^\circ\text{C}$	$T = 538^\circ\text{C}$	$T = 25^\circ\text{C}$	$T = 538^\circ\text{C}$	$T = 25^\circ\text{C}$	$T = 538^\circ\text{C}$	$T = 25^\circ\text{C}$	$T = 538^\circ\text{C}$	$T = 25^\circ\text{C}$	$T = 538^\circ\text{C}$	$T = 25^\circ\text{C}$	$T = 538^\circ\text{C}$
Hot forged	531	352	668	386	26	33	72	85	85	93				
Hot rolled	580	400	718	469	26	35	69	85	85	97				

*Rockwell Hardness—Rockwell B Scale, Ball Indenter $1/16"$, 100 kg load.

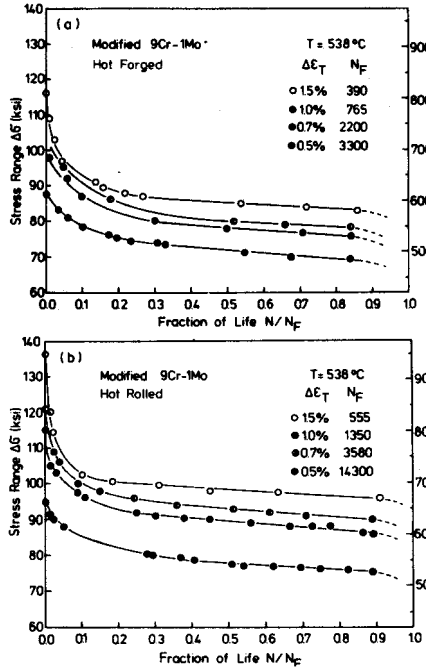


Fig. 2: Cyclic stress response curves at different strain amplitudes for (a) the hot forged material and (b) the hot rolled material

curves of the two materials shows that the stress range at a given fraction of life is always higher for the hot rolled material. The period of rapid initial softening in terms of fraction of lifetime is independent of the applied strain range and takes some 30% of the total lifetime for both processing conditions. The amount of initial softening is a function of the applied strain range and is greater for the hot rolled material at all strain ranges applied. The period of gradual softening in terms of the fraction of total life has approximately the same value for a high strain range and a short test duration as it has for a small strain range and a long test duration. Furthermore there appears to be no significant difference in the period of gradual softening between the hot forged and the hot rolled material.

Fatigue life behaviour

The effect of processing, i.e. hot forged vs. hot rolled, on the HTLCF life of the modified 9Cr-1Mo is demonstrated in Fig. 3. It is clearly shown that for a given total strain range

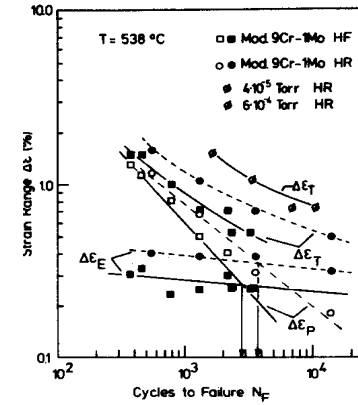


Fig. 3. Fatigue life as a function of strain range at 50% of the cycles to failure for the hot forged and hot rolled materials.

$\Delta\epsilon_T$ the hot rolled material has a longer lifetime than the hot forged material and increasingly more so as the strain range decreases. Also included in this plot are results of vacuum fatigue tests of the hot rolled material. These results demonstrate the pronounced effect of the environment on the HTLCF properties of the modified 9Cr-1 Mo.

Also plotted in Fig. 3 are the elastic and plastic portions of the strain range vs lifetime for the two processing histories. It has been proposed [8] that the following relation exists between the strain amplitude, $\Delta\epsilon_T$, and the number of cycles to failure, N_F :

$$\frac{\Delta\epsilon_T}{2} = \frac{\sigma'_f}{E} (N_F)^b + \epsilon'_f (N_F)^c \quad (1)$$

σ'_f , ϵ'_f , b and c are the fatigue strength coefficient, the fatigue ductility coefficient, the fatigue strength exponent and fatigue ductility exponent, respectively. Using a least squares fit for the hot forged material in these tests at 50% lifetime

$$\frac{\Delta\epsilon_T}{2} = 0.22 N_F^{-0.06} + 73 N_F^{-0.79} \quad (2a)$$

whereas for the hot rolled material

$$\frac{\Delta\epsilon_T}{2} = 0.32 N_F^{-0.07} + 22 N_F^{-0.59}. \quad (2b)$$

A larger portion of the total strain range is elastic for the hot rolled material. For example, at $\Delta\epsilon_T = 0.5\%$ the ratio of elastic and total strain range is 0.50 for the hot forged material

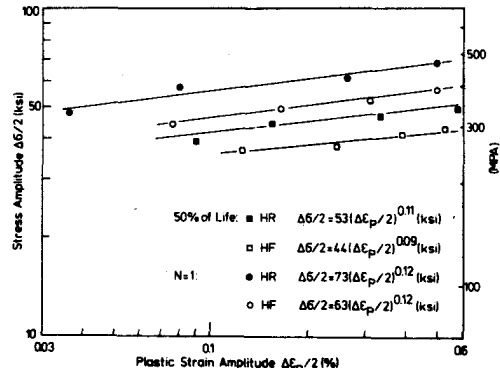


Fig. 4. Cyclic stress-strain properties of hot rolled and hot forged materials

whereas it is 0.64 for the hot rolled material. The hot rolled material also has a higher transition life, i.e. 3800 cycles as compared to 2700 cycles for the hot forged material.

The cyclic stress-strain curves at 50% of the number of cycles to failure are shown in Fig. 4. The higher cyclic strength of the hot rolled material is evident. The equations for the cyclic stress-strain relationship are included in Fig. 4.

The HTLCF properties in terms of only the plastic strain range at 50% lifetime are represented in Fig. 5 where the data points indicated by (7) are taken from Ref. [7]. In view of Coffin's finding that there is no influence of the microstructure on the slope of the plastic strain vs. fatigue life plot [9] it is interesting that in this study the slope depends on

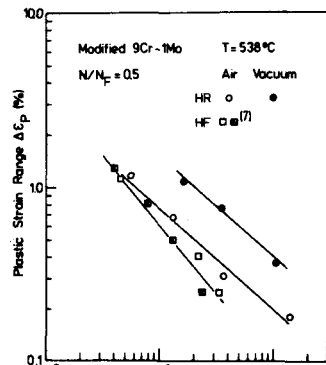


Fig. 5. Fatigue life as a function of plastic strain range at 50% of the cycles to failure.

the processing history. Furthermore, based on Coffin's results [10], one would expect a shallower slope for the vacuum tests. This will be discussed in more detail in a later section.

Metallurgical analysis

Only $M_{23}C_6$ carbide and α -Fe were identified in the as-received materials by X-ray diffraction analysis. The lattice parameter of the complex FCC carbide $M_{23}C_6$ was found to be 10.64 Å and was independent of processing history. X-ray diffraction analysis was also performed on extracted carbides from specimens which had been cycled to failure at a total strain range of 0.5%. However, there was no evidence that a new phase formed during cyclic deformation at 538°C or that the lattice parameter of the $M_{23}C_6$ carbide had changed.

Transmission electron micrographs of as received and fatigued microstructures are shown in Fig. 6(a)–(d). In Fig. 6(a) and (c) the as-received conditions of the hot rolled and hot forged materials are compared. The microstructures consist primarily of packets of parallel laths containing a high density of dislocations. In comparing the two processing histories the mean width of the laths is approx. 0.8 μm for the hot forged material and 0.4 μm for the hot rolled material. In both materials large precipitates are observed lying along prior austenite grain boundaries and lath boundaries. These precipitates are $M_{23}C_6$

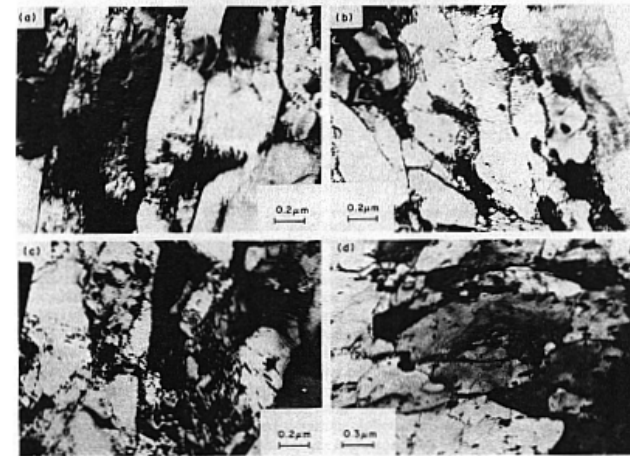


Fig. 6. Transmission electron micrographs of hot rolled material (a) as-received and (b) after cycling at a total strain range of 0.5%; also of the hot forged material (c) as-received and (d) after cycling at a total strain range of 0.5%.

carbides as was revealed by X-ray analysis. In addition the hot rolled material also showed precipitation occurring in the interior of the laths. Since those precipitates possess the same shape as the carbides arranged along the boundaries it is believed that they are also of $M_{23}C_6$ type. Their smaller size might be due to a delayed nucleation or a slower, diffusion controlled, growth rate because they cannot benefit from grain boundary diffusion.

Figure 6(b) and (d) show that cycling has a marked effect on the microstructure of hot forged and hot rolled material. The dislocation density appears to have been reduced, the dislocations have moved to cell boundaries. Cycling at $\Delta\epsilon_T = 0.5\%$ also causes the development towards an equiaxed substructure. In addition, small precipitates appear in the grain interior when cyclic deformation is applied over a longer period of time, i.e. 9 h for the hot forged material and 39 h for the hot rolled material. These particles are associated with tangled dislocations. Their elongated shape seems to be similar to those observed in the hot rolled material.

On the basis of these findings and those of Jones [11] it appears that the initial softening is due to a combination of dislocation annihilation and rearrangement and may also in part result for a loss of strength as Mo-C-Mo clusters transfer to Mo-C pairs which leads to a loss of interaction solid solution hardening [11]. The gradual loss of strength following the initial drop is probably associated with precipitate coarsening.

Fractographic analysis

The fracture surfaces of all failed specimens were examined in the scanning electron microscope and no evidence for an intergranular failure was observed. Fatigue striation spacing measurements were made and the results are plotted in Fig. 7 in terms of the fatigue crack propagation rate da/dN vs. the crack length a . It is noted that there is little difference in crack propagation rate between the hot forged and hot rolled material tested in air at $\Delta\epsilon_T = 10\%$. Again, a pronounced effect occurs when testing is performed in vacuum. At constant crack length the crack growth rate is a function of the applied strain range and increases with increasing $\Delta\epsilon_T$.

Examples of the striated areas are illustrated in Fig. 8. Figure 8(a) and (b) show the influence of the environment, i.e. air vs. vacuum, on the striation formation of the hot rolled

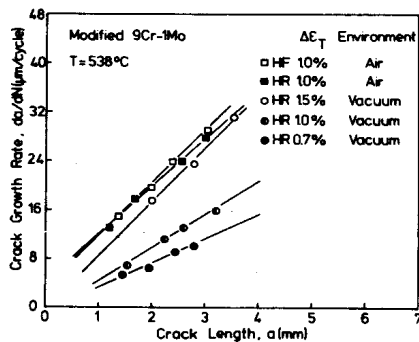


Fig. 7. Crack growth rates determined for striation as a function of crack length

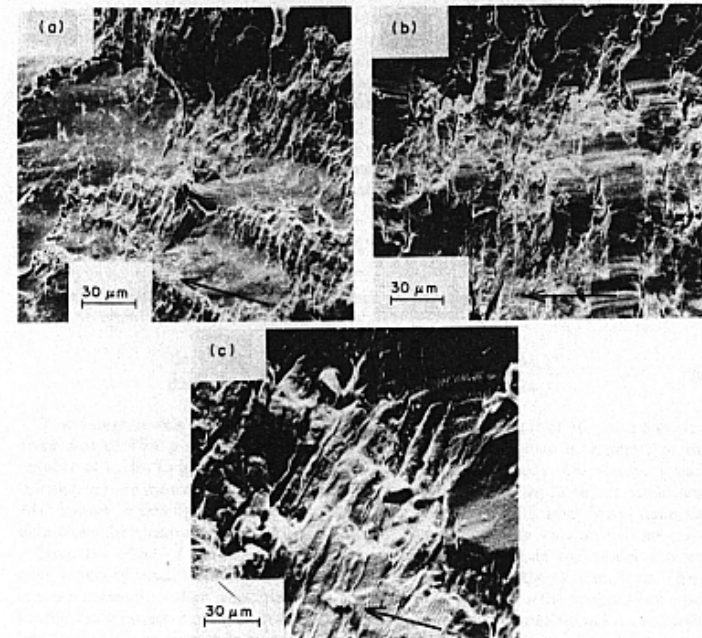


Fig. 8. Striations observed on HTLCF fracture surfaces at a crack length of (a) 1.6 mm (hot rolled material tested in vacuum), (b) 1.2 mm (hot rolled material tested in air) and (c) 1.4 mm (hot forged material tested in air).

material. The photographs are taken at a comparable crack length so that the difference in striation spacing is clearly noted. Also seen are flat regions which indicate that heavy rubbing action took place between the fracture surfaces. Figure 8(c) depicts a striated area of the hot forged material. Note that the individual large striations contain finer markings, an effect also found by Boettner *et al.* [12] in OHFC-copper. These fine markings were interpreted as slip steps introduced during the compression part of the cycle.

After fatigue testing in air or in vacuum, specimens of the hot rolled and hot forged materials were sectioned longitudinally, and micrographs of specimens tested at $\Delta\epsilon_T = 0.7\%$ are shown in Fig. 9 where significant differences between air and vacuum test specimens are noted. For example, the surface of the specimen tested in vacuum was much more rumpled than when tested in air. Also, for the air specimen several crack initiation sites are observed, whereas, for the vacuum specimen no crack was observed except for the fatigue crack itself. The number of cracks per unit length of specimen tested in air was

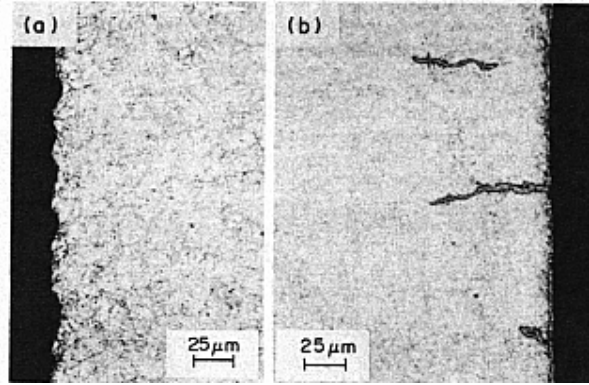


Fig. 9. Surfaced profiles of (a) hot rolled material tested in vacuum at a total strain range of 0.7% and (b) hot forged material tested in air at a total strain range of 0.7%

greater for the hot forged material than it was for the hot rolled material, i.e. 4 cracks per 2 mm vs. 1 crack per 2 mm. After testing in air at a total strain range of 1.5% no difference in number of cracks per unit length between hot forged and hot rolled materials was observed.

DISCUSSION

A finding of interest in this study is that the HTLCF properties of the coarse-grained hot forged material are inferior to those of the fine-grained hot rolled material, with the difference increasing with decreasing strain range. In discussing the cause of this difference it is convenient to separate the low cycle fatigue process into crack initiation and crack propagation stages. A simple model for fatigue crack growth based upon crack tip opening displacement (CTOD) considerations [13] is used to aid in the distinction between crack initiation and crack propagation.

An expression for the CTOD in the linear elastic range is [14]:

$$CTOD = \frac{8}{\pi} \frac{\sigma_y}{E} a \ln \sec \frac{\pi}{2} \frac{\sigma}{\sigma_y}$$

where a is the crack length, σ_y is the yield strength and E is Young's modulus. Since linear elastic conditions are not present during low cycle fatigue this equation must be modified. As an approximation it is assumed that σ_y can be replaced by the ultimate tensile strength. If the material obeys the cyclic stress-strain relation

$$\sigma = k \left(\frac{\Delta \epsilon_p}{2} \right)^n,$$

then the ultimate tensile strength σ_u is given by $k n^n$. In place of Young's modulus the secant modulus, defined as the slope of the straight line connecting the compressive strain point at zero stress with the maximum tensile stress and strain point of the stabilized or average cyclic stress-strain loop. It is assumed that crack growth occurs only in the tensile portion of a loading cycle. Since in the tests of the modified 9Cr-1Mo alloy the elastic strain range is not insignificant with respect to the plastic strain range, the term $\Delta \epsilon_e / 2$ is included in the expression for the secant modulus. In the initial derivation [13] this term was not included since the plastic strain range was taken to be much larger than the elastic strain range. With these modifications equation (3) can now be expressed as

$$CTOD = \frac{8}{\pi} n^n \left(\frac{\Delta \epsilon_p}{2} \right)^{-n} (\Delta \epsilon_p + \Delta \epsilon_e / 2) a \ln \sec \frac{\pi}{2} \left(\frac{\Delta \epsilon_p}{2n} \right). \quad (3b)$$

It is then assumed that the rate of fatigue crack propagation is proportional to the CTOD, or

$$\frac{da}{dN} = \frac{8A}{\pi} n^n \left(\frac{\Delta \epsilon_p}{2} \right)^{-n} (\Delta \epsilon_p + \Delta \epsilon_e / 2) a \ln \sec \frac{\pi}{2} \left(\frac{\Delta \epsilon_p}{2n} \right). \quad (3c)$$

If we integrate this expression between the arbitrarily small limit of 10 μ and a critical crack size of 4500 μ (approx. 60% of the specimen diameter) then an estimate of the number of cycles to grow a crack between these limits can be made. The results of such calculations are shown in Fig. 10 together with the lifetime curves for three test conditions. Also shown in this figure are the computed crack propagation lifetimes based upon the data from the striation measurements shown in Fig. 10 for both vacuum and air tests.

Since the effect of the environment has not been considered in the model a direct comparison of predictions can only be made with the results of the vacuum tests. There is some apparent scatter associated with the three data points for the vacuum tests, but for the strain ranges, employed in the tests, equation (3c) plots reasonably well as a straight line through the vacuum data points in Fig. 10 if a value of $A = 0.25$ is assigned. It is noted that in the plastic range the value of the proportionality constant, A , is much closer to unity than in the elastic range. In fact for large scale plastic deformation of copper single crystals Neumann [15] found an exact equivalency between the crack growth increment and the CTOD. On the other hand, in the elastic range the ratio of the crack growth increment to the CTOD may be of the order of 1:50. The closer agreement between the two quantities in the plastic range suggests that the plastic deformation responsible for the CTOD is concentrated at the crack tip itself as observed by Neumann, whereas in the elastic range the CTOD process is facilitated by plastic deformation on the flanks of the crack away from the tip itself [16].

If we assume that over the strain ranges of interest that both the propagation lifetime and the total lifetime can be represented by straight lines in Fig. 11, then the number of cycles to initiate a 10 μ crack cannot be a straight line on this plot but is curved as shown in Fig. 11. We next examine the relationship between the slopes of these curves to determine the factors affecting the total lifetime slope, f . At a given value of $\Delta \epsilon_p$ we can write

$$N_f = \left(\frac{\Delta \epsilon_p}{C_f} \right)^{-1/f} \quad (4)$$

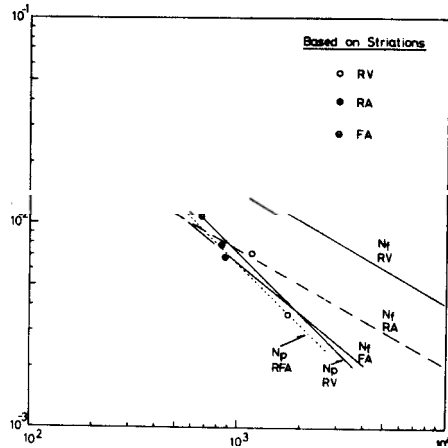


Fig. 10. Predicted crack propagation lifetimes, N_p , compared with propagation lifetimes for vacuum (N_p RV), and air tests (N_p RFA) based on striation measurements. Also shown are the total lifetimes of the hot rolled materials in vacuum and air (N_f RV and N_f RA) and the hot forged material in air (N_f FA).

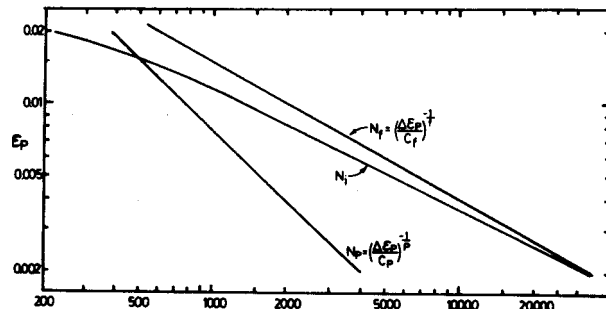


Fig. 11. A comparison of the total life N , the number of cycles spent in propagation, N_p and the number of cycles to initiate a 10μ size crack, N_i .

$$N_p = \left(\frac{\Delta \epsilon_p}{C_p}\right)^{-1/p} \quad (5)$$

and

$$N_i = \left(\frac{\Delta \epsilon_p}{C_i}\right)^{-1/i} \quad \text{and} \quad i = \frac{dN_i}{d(\Delta \epsilon_p)} \quad (6)$$

The first of these expressions is the empirical Coffin-Manson Law, the second expresses the straight-line fit to the calculated propagation lifetimes and the third indicates that the value of N_i at a given value of $\Delta \epsilon_p$ is related to the values of C_i and i which are themselves functions of $\Delta \epsilon_p$. The relationship between N_i , N_p and N_f can be expressed as:

$$N_f = N_p + N_i \quad (7)$$

or

$$\left(\frac{\Delta \epsilon_p}{C_f}\right)^{-1/f} = \left(\frac{\Delta \epsilon_p}{C_i}\right)^{-1/i} + \left(\frac{\Delta \epsilon_p}{C_p}\right)^{-1/p} \quad (8)$$

If we take the derivative of the above equation with respect to $\Delta \epsilon_p$ we obtain:

$$\frac{dN_f}{d\Delta \epsilon_p} = -\frac{1}{f} \frac{N_f}{\Delta \epsilon_p} + \frac{1}{i} \frac{N_i}{\Delta \epsilon_p} = -\frac{1}{p} \frac{N_p}{\Delta \epsilon_p} \quad (9)$$

which leads to the result that at any given $\Delta \epsilon_p$

$$\frac{1}{f} = \frac{N_p}{N_f} \frac{1}{p} + \frac{N_i}{N_f} \frac{1}{i} \quad (10)$$

Therefore the slope of the total lifetime line depends as would be expected upon the relative contributions of the initiation and propagation stages. If the number of cycles to initiation were to be zero, then the value of f would equal that of p . On the other hand if the lifetime were spent in the initiation process only, then would i and f be equal.

With this background we next consider the results of the lifetime tests in air. On Fig. 10 lines representing the total lifetimes for the hot rolled and hot forged materials are shown. Data points based upon the striation measurements are also shown, and a straight line of the same slope as for the vacuum tests has been drawn through these points. Based on the striation data, any difference in fatigue lifetime behaviour must be associated with the initiation stage since the propagation stages were quite similar. Since the slope of the total lifetime line for the hot rolled material tested in air is the same as the slope for the vacuum tests we conclude, based upon equation (10), that at any given value of $\Delta \epsilon_p$ the N_p and N_i cycles have both been reduced by the same percentage. On the other hand, since the slope of the total lifetime line for the hot forged material tested in air is steeper than for the hot rolled material then the proportion of lifetime spent in crack initiation must be less. We attribute the greater ease of crack initiation in the case of the hot forged material to its larger grain size. The specimens tested in air were held at temperature for two hours to allow an oxide to form. In comparing the surface profiles shown in Fig. 9

it appears that this surface oxide can serve as a barrier to slip. However it is a weak barrier, being easily overcome by inhomogeneous plastic deformation in certain favourably oriented grains. A first step in the fatigue failure chain is the rupture of the oxide film. The larger grain size and associated lower yield strength of the hot forged material will facilitate oxide rupture. This oxide rupture could occur as early as the first cycle, dependent upon the plastic strain amplitude. If rupture does not occur in the first cycle, the observed cyclic softening will promote rupture in subsequent cycles due to the associated increase in plastic strain amplitude. Once a crack has been initiated the larger grain size will also facilitate combined Mode I and Mode II growth through the first grain by increasing the crack opening displacement due to a lower yield strength and by reducing the constraints on Mode II deformation as a result of the relatively large distance to the first grain boundary. As the result of these combined effects the number of cycles required to initiate a 10µm crack will be less in the larger grained material.

Conclusions

(1) The HTLCF properties of modified 9Cr-1 Mo ferritic steel are sensitive to grain size, with a larger grain size as in hot forged material leading to inferior fatigue properties as compared to finer-grained hot rolled material.

(2) An air environment degrades the low cycle fatigue properties with respect to vacuum. In the hot rolled material both the initiation and propagation stages were equally affected. In the hot forged material a greater reduction in the number of cycles to initiate a 10 a crack was found, and this reduction was attributable to a larger grain size which facilitated oxide rupture and initial crack formation and growth.

Acknowledgements-The financial support for this investigation provided by the Department of Energy (DOE Contract No. DE-AC02-82ER12065) is gratefully acknowledged. We also express our appreciation to Professor John Morral of the Metallurgy Department at the University of Connecticut for helpful discussions concerning equation (4)-(10). Assistance provided by Mr Jeffrey Bunch is also acknowledged.

REFERENCES

1. Khare A. K. (Ed.) (1983) *Ferritic Steels for High Temperature Applications*. American Society for Metals.
2. Sikka V. K., Ward C. T. and Thomas K. C. (1983) Modified 9Cr-1Mo steel-an improved alloy for steam generator application. In *Ferritic Steels for High Temperature Applications* (Edited by Khare A. K.), pp. 65-84. American Society for Metals.
3. Leslie W. C. (1963) The strengthening of carbon steels by small additions of columbium. *Conference on the Relation Between Structure and Strength in Metals and Alloys*. Teddington, Middlesex.
4. Jones W. B. (1983) Influence of the magneto mechanical effect in testing of inductively heated ferritic steel. NUREG/CR-2649, SAND 82-0752, R7.
5. Enomoto M., Song S. H., Yamada K., Simuzu M. and Kunio T. (1974) A new etching method for prior austenite grain boundaries. *J. Jap. Soc. mech. Engng* 40, 407.
6. Leitnaker J. M., Kleuh R. L. and Laina W. R. (1975) The composition of eta carbide phase in 2 1/4Cr-1Mo steel. *Metall. Trans.* 6A, 1949-1955.
7. Hoffman C. (1982) An investigation of high temperature low cycle fatigue behaviour of materials. Ph.D. dissertation, University of Connecticut.
8. Raske D. T. and Morrow J. (1969) Mechanics of materials in low cycle fatigue testing. *Manual on Low Cycle Fatigue Testing*, ASTM STP 465, pp. 1-25.
9. Tavernalli J. F. and Coffin L. F. (1959) A compilation and interpretation of cyclic strain fatigue tests on metals. *Trans. ASM* 51, 438-450.

10. Coffin L. F. (1972) The effect of high vacuum on the low cycle fatigue law. *Metall. Trans.* 3, 1777-1788.
11. Jones W. B. (1983) The effects of mechanical cycling on the substructure of modified 9Cr-1Mo ferritic steel. In *Ferritic Steels for High Temperature Applications* (Edited by Khare A. K.), pp. 221-235. American Society for Metals.
12. Boettner R. C., Laird C. and McEvily A. J. (1965) Crack nucleation and growth in high strain-low cycle fatigue. *Trans. Metall. Soc. AIME* 233, 379-387.
13. McEvily A. J. (1982) On the quantitative analysis of fatigue crack propagation. *Fatigue Mechanisms: Advances in Quantitative Measurement of Physical Damage*. ASTM STP 811, pp. 283-312.
14. Bilby B. A., Cottrell A. H. and Swinden K. H. (1963) The spread of plastic yield from a notch. *Proc.R. Soc. Lond. A* 271, 304-310.
15. Neumann P. (1969) Coarse slip model of fatigue. *Acta metall.* 17, 1219-1225.
16. Tomkins B. and Biggs W. D. (1969) Low endurance fatigue in metals and polymers. *J. Mater. Sci.* 4, 544-553.